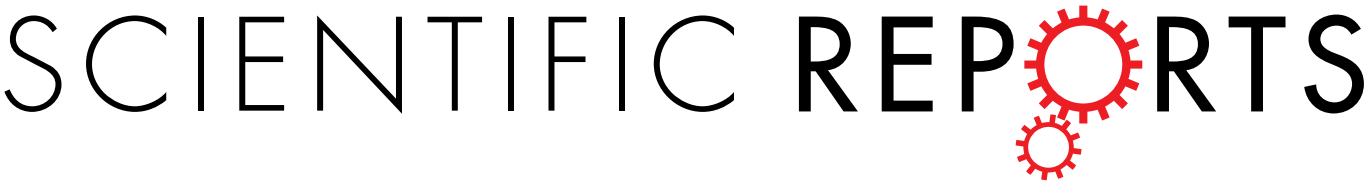

OPEN

Received: 01 December 2016
Accepted: 18 January 2017
Published: 22 February 2017

Mussel-inspired Fluoro-Polydopamine Functionalization of Titanium Dioxide Nanowires for Polymer Nanocomposites with Significantly Enhanced Energy Storage Capability

Guanyao Wang, Xingyi Huang & Pingkai Jiang

High-dielectric-constant polymer nanocomposites are demonstrated to show great promise as energy storage materials. However, the large electrical mismatch and incompatibility between nanofillers and polymer matrix usually give rise to significantly reduced breakdown strength and weak energy storage capability. Therefore, rational selection and elaborate functionalization of nanofillers to optimize the performance of polymer nanocomposites are vital. Herein, inspired by adhesive proteins in mussels, a facile modification by fluoro-polydopamine is employed to reinforce the compatibility of TiO_2 nanowires in the fluoropolymer matrix. The loading of 2.5 vol % *f*-DOPA@TiO_2 NWs leads to an ultrahigh discharged energy density of 11.48 J cm^{-3} at 530 MV m^{-1}, more than three times of commercial biaxial-oriented polypropylene (BOPP, 3.56 J cm^{-3} at 600 MV m^{-1}). A gratifying high energy density of 9.12 J cm^{-3} has also been obtained with nanofiller loading as high as 15 vol % at 360 MV m^{-1}, which is nearly double to that of pure P(VDF-HFP) (4.76 J cm^{-3} at 360 MV m^{-1}). This splendid energy storage capability seems to rival or exceed most of previously reported nano-TiO_2 based nanocomposites. The methods presented here provide deep insights into the design of polymer nanocomposites for energy storage applications.

Electric energy storage plays an indispensable role in modern electronic devices and electric power systems[1–4]. The development of high-energy-storage-density devices is of critical importance to meet the ever-increasing urgent need. Dielectric materials, which possess the intrinsic charge-discharge capability to store and release the electrical energy through dielectric polarization and depolarization, have attracted immense interest for their potential applications in energy storage devices such as capacitors[5–11]. Among numerous dielectric materials, polymer nanocomposites are receiving growing concern because of the advantage combining the merits of ceramics (e.g., high dielectric constant) and polymer (e.g., high breakdown strength and ease of processing)[12–30]. However, the straightforward incorporation of high-dielectric-constant (high-*k*) nanofillers into low-dielectric-constant (low-*k*) polymer matrix might not be an ideal strategy for the increase of energy storage, since the large electrical mismatch between the two components might bring up an inevitable electric field distortion and the resulting reduction of breakdown strength for the nanocomposite[15,21,30].

Development of simple and versatile strategies for modification of inorganic nanofillers has proven to be an effective method to improve their compatibility with the polymer matrices[31,32]. Our previous work has demonstrated that the employment of atom transfer radical polymerization (ATRP) and reversible addition-fragmentation chain transfer (RAFT) polymerization upon the modification of $BaTiO_3$ nanoparticles could significantly improve their inclusion into the ferroelectric polymer matrix[33–39]. However, these

Department of Polymer Science and Engineering, Shanghai Key Laboratory of Electrical Insulation and Thermal Aging, Shanghai Jiao Tong University, Shanghai 200240, China. Correspondence and requests for materials should be addressed to X.H. (email: xyhuang@sjtu.edu.cn)

methods intrinsically suffer from harsh experiment conditions (water-free and oxygen-free), time-consuming, and equipment-requiring drawbacks. Therefore, there is still an urgent need to develop a facile and fast method for the surface modification of nanofillers in the fabrication of polymer nanocomposites. As a burgeoning technology of self-assembled monolayers (SAMs), the dopamine self-polymerization, inspired by the composition of adhesive proteins in mussels, has gained a lot of popularity due to the one-step requirement over the last few years[32,40–48]. The thin surface-adherent polydopamine films can stick to a variety of inorganic and organic materials, by means of catechol-based adhesive compounds.

Herein, TiO_2 nanowires (NWs) are selected rationally as the nanofillers in order to mitigate the field intensification, owing to the balanced dielectric constant of TiO_2 with the ferroelectric polymer matrix[15,21,30] and smaller specific surface of high-aspect-ratio nanowires compared with their nanoparticle counterparts to reduce the surface energy and alleviate the agglomeration of the nanofillers[25,28]. Meanwhile, we also introduce a long fluoro-chain tailed dopamine derivative, *f*-DOPA, to generate corresponding fluoro-polydopamine thin layers upon the pristine TiO_2 NWs. The facile one-step modification guarantees the excellent inclusion of modified TiO_2 NWs in the fluoropolymer matrix, and further facilitates the remarkable improvement of energy storage capability in comparison with pristine polymer matrix and the commercial biaxial-oriented polypropylene (BOPP). Furthermore, the elaborate functionalization of TiO_2 NWs would also make for the reduction of temperature dependence on dielectric properties, which scarifies the reliability and performance of the dielectric materials. More striking is that high energy densities could also be achieved even at a rather low electric field, benefiting from the high loadings of attentively prepared nanofillers. We could then establish a comprehensive understanding upon the influence of aborative modification of nanofillers on the following optimization of the electric properties of polymer nanocomposites from all aspects of their properties. The results and methods presented here will provide deep insights into the design and fabrication of polymer nanocomposites for dielectric and energy storage applications at both low and high electric fields.

Experimental Section

Materials. Poly(vinylidene fluoride-co-hexafluoropylene) (P(VDF-HFP)) with 15% HFP was supplied by Solvay Plastics (Shanghai, China). Titanium dioxide nanopowder (TiO_2, P25, $\geq$99.5%) was purchased from Sigma-Aldrich. 3,4-dihydroxy-*L*-phenylalanine (*L*-DOPA, 99%) and *p*-toluenesulfonic acid monohydrate (98%) were provided by Aladdin (China). 1*H*, 1*H*, 2*H*, 2*H*-perfluoro-1-decanol (TCI, 96%) were both purchased from Tansoole (China). Other chemicals or reagents were purchased from Sinopharm Chemical Reagent Co., Ltd. (China) and Tansoole (China).

Synthesis of 1*H*, 1*H*, 2*H*, 2*H*-heptadecafluorodecyl 2-amino-3-(3,4-dihydroxyphenyl)propanoate (*f*-DOPA). The synthesis of *f*-DOPA was accomplished according to previous literatures[48]. A suspension of *L*-DOPA (3.94 g, 20 mmol), 1*H*, 1*H*, 2*H*, 2*H*-perfluoro-1-decanol (9.28 g, 20 mmol), and *p*-toluenesulfonic acid monohydrate (3.80 g, 20 mmol) in toluene (100 mL) was reflux under a N_2 atmosphere for 48 h, using a Dean-Stark trap to aezotropically remove water. After cooling to room temperature, the toluene was evaporated under vacuum. The gel-like solid residue was washed with saturated $NaHCO_3$ aqueous solution and extracted with ethyl acetate. The ethyl acetate solution was further washed with brine for several times. Then the solution was dried over anhydrous $MgSO_4$ for several hours and filtered. After evaporation, the raw product was dissolved in a small amount of hot ethyl acetate and crystallized from petroleum ether (60–90 °C). Yield: 8.17 g, colorless solid (63.52%).

Surface Modification of Nanowires. The TiO_2 NWs were synthesized by employing hydrothermal method described in previous literatures[27]. Then, the dopamine derivative *f*-DOPA was utilized to modify the surface of the pristine TiO_2 NWs. In a typical process, 3 g TiO_2 NWs were dispersed in 80 mL Tris-HCl buffered solution (pH = 8.5) and ultrasonicated for 1 h. Meanwhile, 4 mmol *f*-DOPA was dissolved in 40 mL 2-propanol. Then, the 2-propanol solution of *f*-DOPA was added dropwise into the aforementioned aqueous solution of TiO_2 NWs under stirring at 60 °C. The mixture was further stirred for 48 h. With the spontaneous deposition of adherent polydopamine derivative film on the surface of nanowires, the color of the mixture was finally changed to black. After extracting from the solution with centrifugation, the nanowires were washed with deionized water and water for several times until the supernatant was nearly colorless. These surface modified nanowires were denoted as *f*-DOPA@TiO_2 NWs.

Fabrication of P(VDF-HFP)-based Nanocomposite Films. The typical process for the fabrication of P(VDF-HFP)-based nanocomposite films was described as follows: The functionalized TiO_2 nanowires were first ground thoroughly and dispersed in DMF by ultrasonication for 1 h. After the addition of given amount of P(VDF-HFP), the mixture was stirred vigorously for 24 h to make it stable and homogenous. The mixture was cast into films on a glass plate with a facile scraper, and then heated at 40 °C to facilitate the evaporation of DMF. After being dried in vacuum at 40 °C for 12 h to remove the remaining trace solvent, the cast films were heated at 200 °C for several minutes and then quenched in ice water immediately. The quenched films were peeled from the glass substrates and dried at 40 °C for another 12 h. The typical thickness of these nanocomposite films is about 15 μm. Nanocomposites with different volume fractions (2.5%, 5%, 10%, and 15%) of *f*-DOPA modified TiO_2 NWs were prepared.

Characterization. The ^1H, ^{13}C, and ^{19}F nuclear magnetic resonance (NMR) spectra were recorded on a AVANCE III HD 400 spectrometer (Bruker, USA). The morphology of the nanowires and samples was characterized with scanning electron microscopy (SEM, Nova NanoSEM 450, FEI, USA) and transmission electron microscopy (TEM, JEM-2010, JEOL, Japan). The cross-section SEM images of nanocomposite films were prepared by fracturing the films in liquid nitrogen. The samples for the TEM were prepared by dropping a few drops

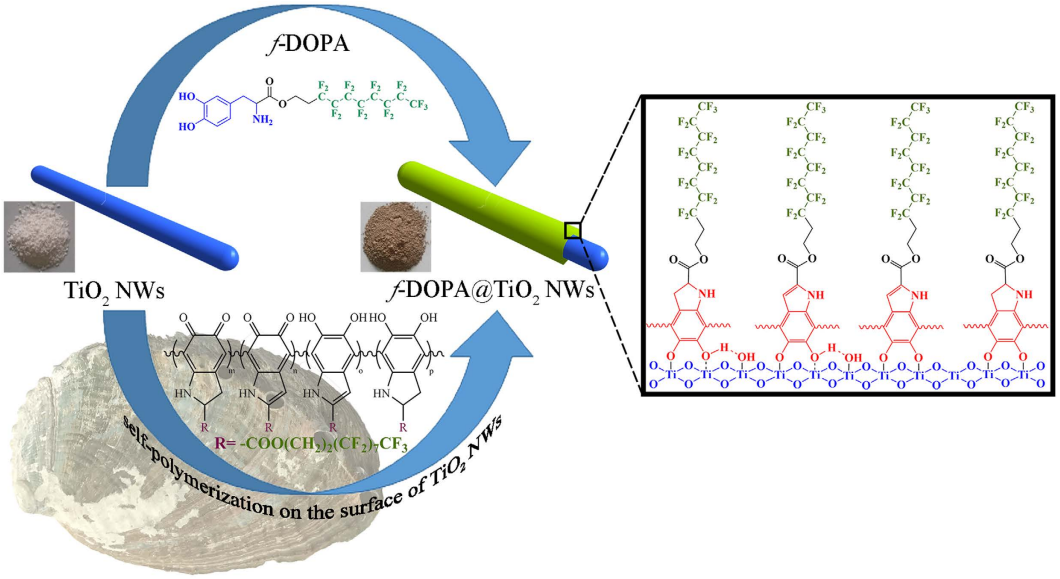

Figure 1. Schematic illustration of the preparation process for *f*-DOPA@TiO_2 NWs. Inset is a photograph of a mussel.

of the sample solution on a carbon-coated cooper grids and air-dried before measurement. The Fourier-transform infrared spectroscopy (FT-IR) of the pristine and surface modified nanowires was performed by PerkinElmer Paragon 1000 spectrometer with the range of 4000–400 cm^{-1}. X-ray photoelectron spectra (XPS) of the nanowires were conducted using an Axis UltraDLD spectrometer (Shimadzu-Kratos Analytical, UK) with a monochromated Al Kα source. Thermogravimetric analysis (TGA) of nanowires was performed with NETZSCH TG209 F3 with a heating rate of 20 °C min^{-1} in a nitrogen flow (20 mL min^{-1}). Both sides of the proposed nanocomposite films were sputtered by copper with diameter of 12 mm for the measurements of dielectric properties. The dielectric constant and loss tangent of the samples were measured with a Novocontrol Alpha-A high resolution dielectric analyzer (GmbH Concept 40) with the frequency range 10^{-1}–10^7 Hz at room temperature and various temperature (−50 °C–150 °C). The electric breakdown tests were carried out with a dielectric strength tester at a ramping rate of 500 V s^{-1} (Shanghai Juter High Voltage Electrical & Equipment Co., Ltd., China). All the samples used for breakdown strength have a thickness of around 15 μm. Electric displacement-electric field (*D*-*E*) loops and two probe current-voltage (I–V) measurements were conducted by a Precision Multiferroic Materials Analyzer equipped with Precision 10 kV HVI-SC and Trek MODEL 609B (Radiant Inc.). A layer of copper was evaporated on both sides of the samples to serve as electrodes (3 mm in diameter).

Results and Discussion

Preparation and Characterization of the Pristine and Surface Modified Nanowires. In Fig. 1, the general synthetic route to prepare the dopamine derivative modified *f*-DOPA@TiO_2 NWs is depicted. As shown in Fig. 1, the white TiO_2 powders turned into brown after the modification of long fluoro-chain tailed dopamine derivative caused by the adhesion of corresponding fluoro-polydopamine layers. The structure of *f*-DOPA was confirmed by NMR spectra (See Supplementary Figs S1–S6). Compared with ^{1}H NMR spectrum of *L*-DOPA (See Supplementary Fig. S1), the splitting multiplet peaks of methylene group on the catechol between 2.5 ppm and 3.0 ppm were shifted to 4.29 ppm in the ^{1}H NMR spectrum of *f*-DOPA (see Supplementary Fig. S3). Besides, the multiplet peaks lined in the range of 2.50 ppm to 2.75 ppm can be ascribed to the two methylene groups of 1*H*, 1*H*, 2*H*, 2*H*-perfluoro-1-decanol. As shown in Supplementary Figs S4 and S5, the dense and weak multiplet peaks between 120 ppm and 105 ppm in the ^{13}C NMR spectrum of *f*-DOPA can be attributed to the carbon signals of the long fluorocarbon chain, which were attenuated by the attached fluorine atoms in comparison with the normal carbon signals[49]. The ^{19}F NMR spectrum of *f*-DOPA gave a further detailed evidence for existence of fluorine atoms (see Supplementary Fig. S6). All these results indicate that the esterification of *L*-DOPA by 1*H*, 1*H*, 2*H*, 2*H*-perfluoro-1-decanol was successful by adopting *p*-toluenesulfonic acid as the catalyst and toluene as the solvent.

SEM and TEM were carried out to characterize the morphology of nanowires and polymer nanocomposites. The free-standing TiO_2 NWs with several micrometers in length are shown in Supplementary Fig. S7. The aspect ratio distribution of TiO_2 NWs summarized in Supplementary Fig. S8 demonstrates that the length-diameter ratio mainly lies in the range of 19–23. As shown in Fig. 2, the distinct thin amorphous layers with ~11 nm thickness reveal the successful deposition and coating of fluoro-polydopamine on the nanowire surface, which facilitate the subsequent dispersion of nanowires in the fluoropolymer matrix. Moreover, the EDX elemental mapping images in Supplementary Fig. S9 also validate the successful attachment of proposed fluoro-polydopamine.

XPS and FT-IR are employed to further demonstrate the successful coating of fluoro-polydopamine layer on the surface of the pristine TiO_2 NWs. As shown in Fig. 3, the presence of N 1 s peak at a binding energy of 400 eV in the XPS spectra confirmed that the nitrogen-containing dopamine derivative had been adhered on the

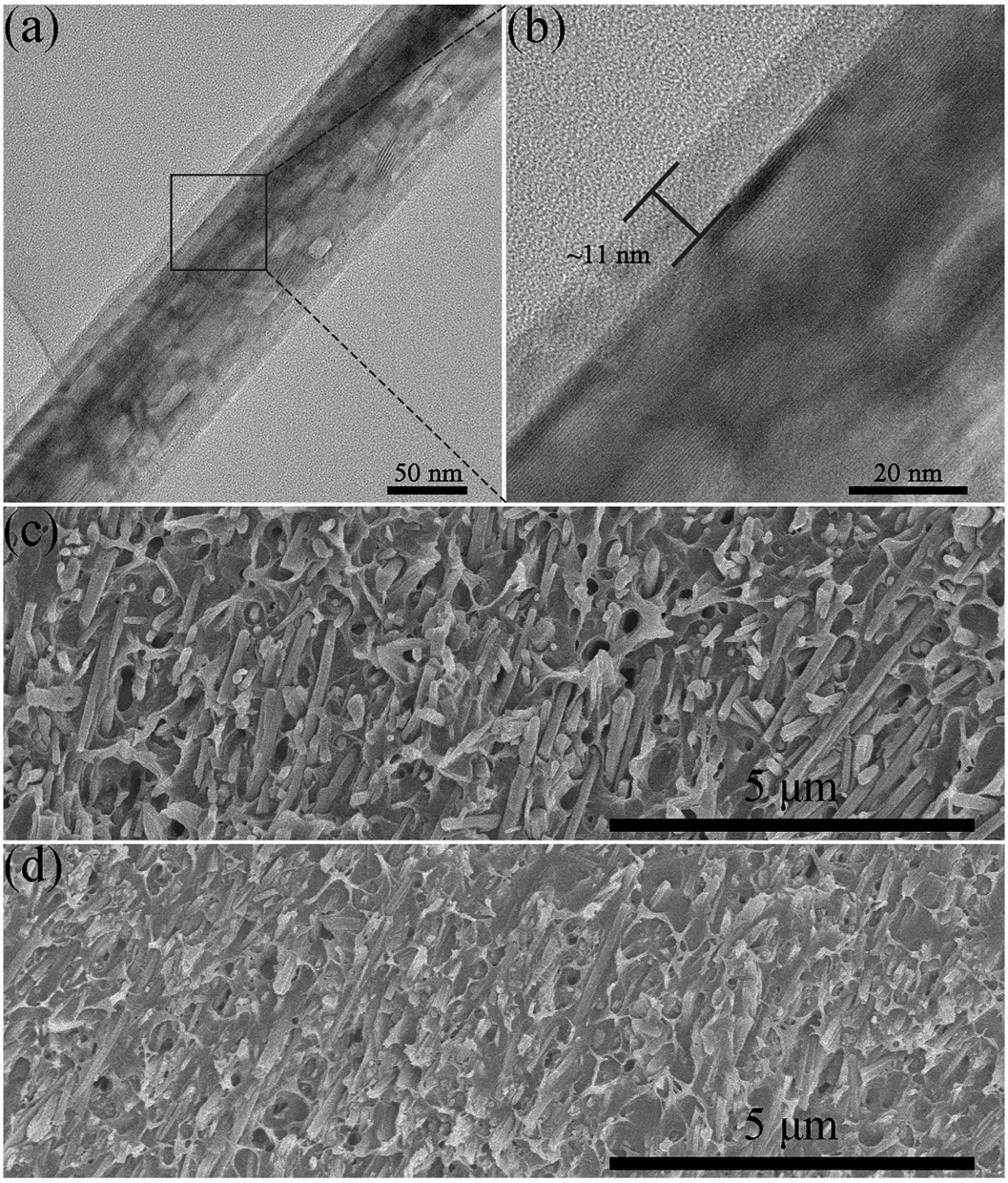

Figure 2. (**a**,**b**) TEM images of *f*-DOPA@TiO_2 NWs. SEM images of freeze-fractured cross-section surfaces of P(VDF-HFP)-based nanocomposites with 15 vol % loading of (**c**) *f*-DOPA@TiO_2 NWs and (**d**) TiO_2 NWs.

nanowire surface through the oxidative self-polymerization of dopamine derivative. Furthermore, the apparent F 1 s peak at the binding energy of 689 eV gave a more solid evidence for the existence of fluorinated polydopamine derivative on the surface of *f*-DOPA@TiO_2 NWs. Moreover, from the FT-IR spectra in Supplementary Fig. S10, obvious changes between 3000 and 2800 cm^{-1} can be observed after the dopamine derivatives functionalization, which can be ascribed to the C-H (methyl and methylene) stretching vibrations in the polydopamine derivatives. Meanwhile, the specific bending vibrations of C-H (methyl and methylene) are located in the range of 1500–1000 cm^{-1} for the surface modified nanowires. The intensity of the broad peak around 3500 cm^{-1} also became more remarkable after the modification in comparison with the pristine nanowires, resulting from the incorporation of amine group in *f*-DOPA.

The difference of composition and thermal stability between the pristine and surface modified nanowires was investigated by TGA. As shown in Supplementary Fig. S11, the total weight loss of the pristine TiO_2 from 50 to 800 °C was about 0.41 wt%, indicating the successful high-temperature calcination of $H_2Ti_3O_7$ precursor[50]. However, the removal of the water inside the precursor would inevitably bring about the defects, which benefit the following surface modification. The weight loss of *f*-DOPA@TiO_2 NWs was notably increased to 7.68 wt%, further affirming the successful anchoring of fluoro-polydopamine layers.

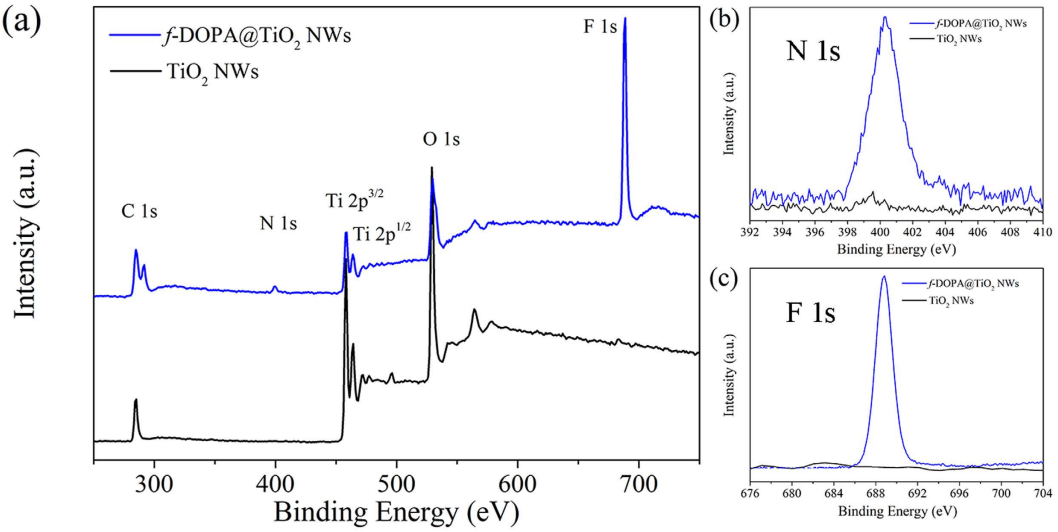

Figure 3. (**a**) XPS spectra of the pristine and surface modified TiO_2 NWs. High-resolution N 1s (**b**) and F 1s (**c**) regions of TiO_2 NWs before and after surface modification.

Microstructure of P(VDF-HFP)-based Nanocomposites. P(VDF-HFP)-based nanocomposite films with certain volume fractions (2.5%, 5%, 10% and 15%) of modified TiO_2 NWs were prepared by solution blending method, respectively. As a control, Fig. 2c and Supplementary Fig. S12 present the SEM images of freeze-fractured cross-section surface of the nanocomposites with 15 vol % raw TiO_2 NWs. Obvious agglomeration of nanowires could be observed. Besides, some nanowires were found to stretch outside the polymer matrix, indicating the weak compatibility between the pristine nanowires and polymer matrix. Such phenomenon was dramatically averted by adopting the surface modified nanowires. As shown in Fig. 2d, the fluoro-polydopamine coated nanowires are homogeneously distributed in the polymer matrix. After modification, these nanowires are buried well inside the polymer matrix. Meanwhile, the tails of these functionalized nanowires rarely stretch outside the cross-section surfaces. All these aforementioned microstructure characteristics indicate that the fluoro-polydopamine functionalized TiO_2 NWs possess excellent compatibility with the fluoropolymer matrix.

Dielectric Properties of the P(VDF-HFP)-based Nanocomposites. The large electrical mismatch between conventional high-*k* nanofillers (for instance, $BaTiO_3$, $Ba_xSr_{1-x}TiO_3$, and $PbZr_xTi_{1-x}O_3$) and ferroelectric polymers usually gives rise to a highly distorted electric field and leads to a significantly reduced effective breakdown strength of the nanocomposites[16,24–26,51]. Herein, in order to maintain the high breakdown strength of polymer matrix and the flexibility of the composite films, the low volume fraction of *f*-DOPA@TiO_2 NWs (under 15 vol %) are utilized as dopants in the ferroelectric P(VDF-HFP). The enhanced dielectric constant and restrained dielectric loss of the proposed nanocomposites over the polymer matrix are shown in Fig. 4a. Apparently, the dielectric constants of the nanocomposites possess a gradual increase with the increased loading of nanowires, resulting from higher dielectric constant of the TiO_2 NWs relative to the polymer matrix[15,30]. By contrastively evaluation with the nanocomposites with 15 vol % raw TiO_2 NWs as the reference, it can be concluded that the dielectric loss of the nanocomposites is drastically supressed, especially at the low frequencies ($<10^4$ Hz), by adopting the fluoro-polydopamine modified TiO_2 NWs. This splendid characteristic of these nanocomposites with *f*-DOPA@TiO_2 NWs in comparison with those with pristine TiO_2 NWs can be ascribed to the restrained interfacial polarization at low frequencies. At low frequencies, the proposed nanocomposites show slight increase of dielectric loss tangent in comparison with the pure polymer because of the interfacial polarization[33,52,53]. It should be noted that, in high frequencies, all the nanocomposites show lower dielectric loss tangent compared with the neat polymer. This phenomenon can be attributed to the enhanced interfacial interaction between the modified TiO_2 NWs and the polymer matrix, which restricts the dipolar polarization of the P(VDF-HFP) macromolecular chains. Moreover, the dielectric loss tangents of the proposed nanocomposites show little variation in comparison with the pristine P(VDF-HFP), further implying that the surface modified TiO_2 NWs are well dispersed in the polymer matrix.

In order to assess the dielectric performance of the proposed nanocomposites comprehensively, the dielectric properties of the nanocomposites with 15 vol % pristine TiO_2 NWs and *f*-DOPA@TiO_2 NWs, as well as the neat polymer, have been characterized as a function of frequency and temperature. As shown in Fig. 4b, the proposed nanocomposites exhibit typical ferroelectric behavior with the dielectric peak shifting gradually to higher temperature as frequency increases just like the pristine P(VDF-HFP) (see Supplementary Fig. S13a). Obvious broad dielectric peaks of these nanocomposites could be ascribed to the kinetics associated with the dipolar glass freezing transition[12]. The major peak at about −30 °C in the dielectric loss spectra results from the glass transition of the pure polymer. As shown in Fig. 4b and Supplementary Fig. S13b, the elaborately modified *f*-DOPA@TiO_2 NWs show inferior elevation of dielectric constant compared with raw TiO_2, resulting from the robust shell to hamper the role of inorganic TiO_2 inside the host matrix. However, further investigation of dielectric loss

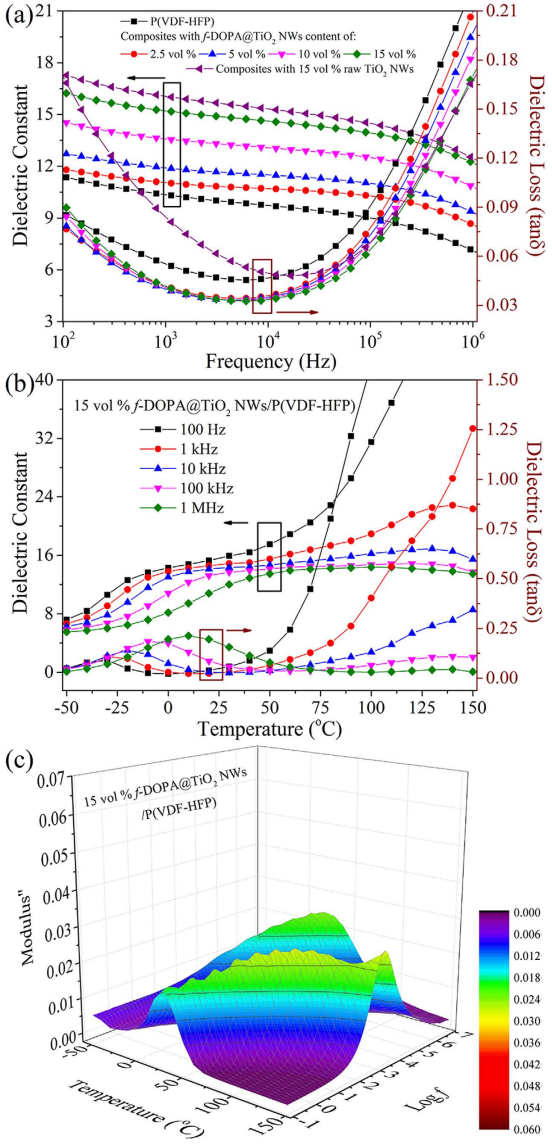

Figure 4. (**a**) The dielectric constant and dielectric loss (tan δ) as a function of frequency at room temperature for *f*-DOPA@TiO_2 NWs/P(VDF-HFP) nanocomposites. (**b**) Temperature-dependent dielectric spectra of *f*-DOPA@TiO_2 NWs/P(VDF-HFP) nanocomposites. (**c**) Frequency dependent of imaginary electric modulus at various temperature of P(VDF-HFP)-based nanocomposites with 15 vol % of *f*-DOPA@TiO_2 NWs.

demonstrates that *f*-DOPA@TiO_2 NWs possess superior circumvention of interfacial polarization and restriction of movement of macromolecular chains at high temperature and low frequency.

To further explore the temperature response and temperature sensitivity of dielectric properties of the proposed nanocomposites, Fig. 4c and Supplementary Fig. S13c,d illustrate the frequency dependence of the imaginary part of the electric modulus (M'') of these aforementioned nanocomposites and neat polymer at various temperature, respectively. For composite systems, the interfacial polarization, also known as Maxwell-Wagner-Sillars (MWS) polarization, represents the accumulation of charge carriers at the interface of heterogeneous systems[30,54]. The explanation of MWS polarization would contribute to analyze the bulk relaxation behaviors of the proposed nanocomposites[30,55]. Two relaxation processes could be observed in these curves. The segmental motions of the amorphous region in the polymer matrix result in the relaxation peaks at high frequency[30,56]. The peaks occurring at low frequency and high temperature (above 50 °C) are associated with the MWS polarization of P(VDF-HFP) (see Supplementary Fig. S13c)[30,56]. With the increase of temperature, these peaks exhibit a gradual shift to the higher frequency, resulting from the decrease of relaxation time aroused by the enhanced mobility of charge carriers at high temperature. For those composite systems, the addition of TiO_2 cripples the relaxation intensity of MWS polarization effectively, suggesting that the incorporation of TiO_2 could greatly circumvent the charge aggregation at the boundaries of crystal and amorphous parts inside the polymer matrix. As discussed above, the thermo-sensitivity of the polymer nanocomposites subsides effectively upon the

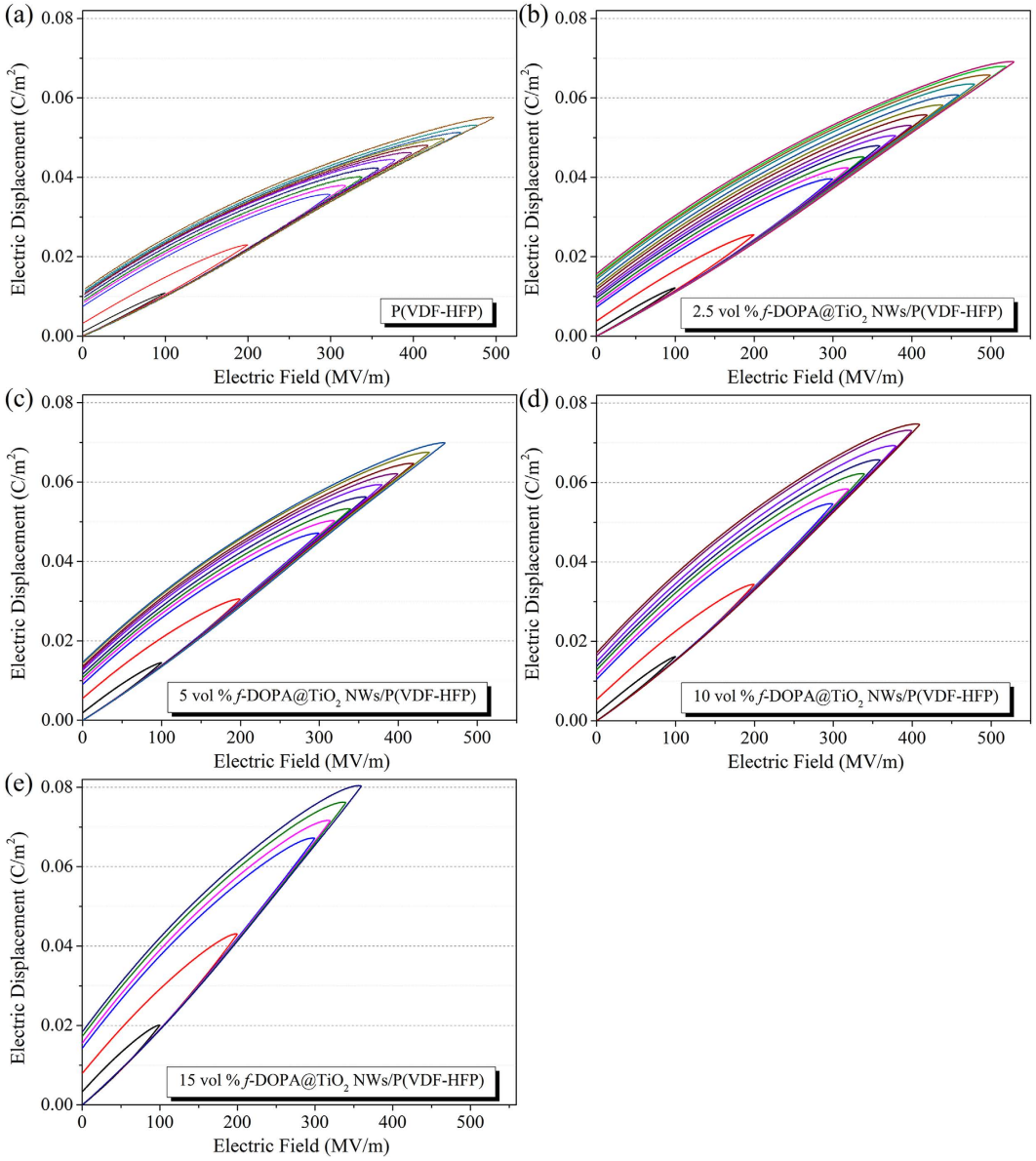

Figure 5. *D-E* loops under unipolar electric fields of 100 Hz for (**a**) pure P(VDF-HFP) and P(VDF-HFP)-based nanocomposites with (**b**) 2.5 vol %, (**c**) 5 vol %, (**d**) 10 vol %, and (**e**) 15 vol % of *f*-DOPA@TiO_2 NWs.

introduction of elaborately functionalized *f*-DOPA@TiO_2 NWs in comparison with pristine polymer and those nanocomposites with raw nanowires.

Energy Storage Capability of P(VDF-HFP)-based Nanocomposites. Generally, the energy density (U_e) of a dielectric material is given by[21],

$$U_e = \int EdD \tag{1}$$

where E is the applied electric field, and D is the electric displacement. Therefore, the energy density is related to the polarization and applied electric field. Generally, the energy storage capability of the dielectric materials can be evaluated from *D-E* loops by a modified Sawyer-Tower circuit. Typical *D-E* loops of pristine P(VDF-HFP) and a series of P(VDF-HFP)-based nanocomposites with *f*-DOPA@TiO_2 NWs are presented in Figs 5 and 6a. Obviously, relatively higher dielectric constant of the modified TiO_2 NWs in comparison with the neat polymer matrix gives rise to the increased electric displacement for the proposed nanocomposites. Nevertheless, it can also be observed that the remnant polarizations presented in these *D-E* loops of these nanocomposites increase with the loading of the TiO_2 NWs, due to the higher remnant polarization of the nanofillers than that of the polymer matrix. Typically, the high remnant polarization of the dielectric materials would result in the reduction of the discharged energy because of the decreased integrated area of *D-E* loops. Thus, low volume fractions of TiO_2

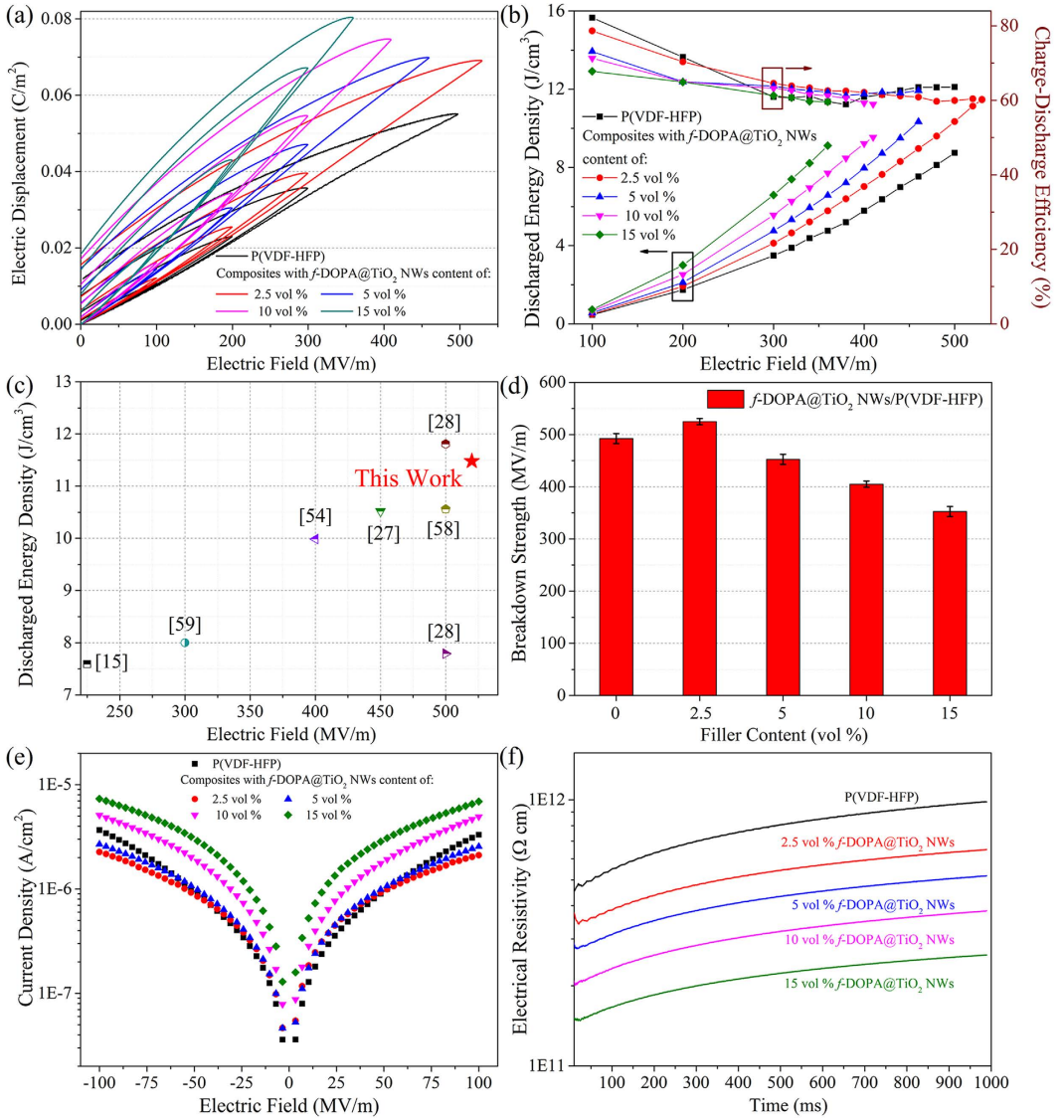

Figure 6. (**a**) *D-E* loops under unipolar electric fields of 100 Hz for *f*-DOPA@TiO_2 NWs/P(VDF-HFP) nanocomposites with different filler concentrations. (**b**) The discharged energy densities and charge-discharge efficiency of P(VDF-HFP)-based nanocomposites with different volume fractions of *f*-DOPA@TiO_2 NWs under varied applied fields. (**c**) Discharged energy densities of 2.5 vol % *f*-DOPA@TiO_2 NWs/P(VDF-HFP) and other nano-TiO_2 related polymer nanocomposites reported in previous literatures in the range of 220 MV m^{-1} to 530 MV m^{-1}. (**d**) Breakdown strength of the P(VDF-HFP)-based nanocomposites at varied volume fractions of *f*-DOPA@TiO_2 NWs. (**e**) Leakage current density of *f*-DOPA@TiO_2 NWs/P(VDF-HFP) nanocomposites with different filler concentrations at varied applied electric field. (**f**) Electrical resistivity of P(VDF-HFP)-based nanocomposites with different volume fractions of *f*-DOPA@TiO_2 NWs under an electric field of 100 MV m^{-1}.

NWs (under 15 vol %) were added as dopants in the fabrication of the proposed polymer nanocomposites. As demonstrated in the Fig. 5, slim *D-E* hysteresis loops with low remnant polarization are depicted evidently in the nanocomposites, denoting their relatively high energy efficiency discussed below.

The energy densities of the proposed nanocomposites derived from the *D-E* hysteresis loops and equation 1 are summarized in Fig. 6b and Supplementary Fig. S14. Obviously, the discharged energy densities of P(VDF-HFP)-based nanocomposites exhibit a gradual increase with the increasing loading of modified TiO_2 NWs and applied electric fields, in concert with the trend of the total stored energy densities (see Supplementary Fig. S14). For example, the total stored energy densities of the nanocomposite with 2.5 vol % *f*-DOPA@TiO_2 NWs is 19.07 J cm^{-3} at 530 MV m^{-1}, much higher than that of pure P(VDF-HFP) (13.75 J cm^{-3} at 500 MV m^{-1}). The nanocomposite with 2.5 vol % *f*-DOPA@TiO_2 NWs discharges an ultrahigh energy density of 11.48 J cm^{-3} at 530 MV m^{-1}, more than three times of the commercial biaxial-oriented polypropylene (BOPP, 3.56 J cm^{-3} at 600 MV m^{-1})[57]. More notably, the nanocomposite with 15 vol % nanowires also possess a striking high energy density of 9.12 J cm^{-3} at 360 MV m^{-1}, nearly doubled to that of pure P(VDF-HFP) at the same electric field (4.76 J cm^{-3}). In order to manifest the outstanding energy storage capabilities of these

nanocomposites, the discharged energy densities of proposed nanocomposite with 2.5 vol % *f*-DOPA@TiO_2 NWs and other previously reported polymer nanocomposites (mostly nano-TiO_2 based) are summarized in Fig. 6c and Supplementary Fig. S15. The discharged energy density of proposed nanocomposite with 2.5 vol % *f*-DOPA@TiO_2 at 530 MV m^{-1} seems to rival or exceed those of previously fabricated nano-TiO_2 based nanocomposites in the range of 220–500 MV m^{-1} [15,27,28,54,58,59]. These amazing results indicate their splendid potential as energy storage materials at both low and high electric fields.

For desirable energy storage capacitors, the energy storage efficiency (η) is also of great importance since the low energy storage efficiency can cause energy losses and reduce the lifetime of the materials. In order to maintain a high energy efficiency, one feasible approach is to suppress the dielectric loss tangent and leakage current density by improving the compatibility between the nanofillers and polymer matrix in the nanocomposites. Figure 6b shows the high efficiencies of the proposed nanocomposites by introducing dopamine derivative functionalization upon the TiO_2 NWs. After the incorporation of modified TiO_2 NWs, the energy efficiencies (discharged energy/total stored energy) are confronted with a gradual decrease with the increasing nanowire loadings due to the conduction loss before the approximate plateau above 300 MV m^{-1} [25,60]. It's heartening that the P(VDF-HFP)-based nanocomposites with *f*-DOPA@TiO_2 NWs bear the efficiencies of ca. 60% at each highest tolerable electric fields, just a little lower than that of neat polymer (ca. 63.6%) at 500 MV m^{-1}. This can be understood from the similar hysteresis in the polarization of the nanocomposites in comparison with that of the pristine polymer. Namely, the elaborate modification of the TiO_2 NWs paves the way of maintenance of the high energy efficiencies, even at the maximum loading of 15 vol %. The much improved efficiencies can also be attributed to the synergistic effect of the significantly reduced leakage current densities discussed below.

Dielectric breakdown strength (E_b) is of tremendous importance for the practical applications of dielectric materials. For a linear dielectric material, the equation 1 turns out to be[2,21]:

$$U_e = 1/2\varepsilon_r\varepsilon_0 E_b^2 \quad (2)$$

where ε_r is the relative dielectric constant, ε_0 the vacuum permittivity (8.8542×10^{-12} F m^{-1}). Therefore, the energy storage of the dielectric materials is strongly dominated by E_b. Previous literatures have demonstrated that balancing dielectric constant by a rational selection of nanofiller and polymer matrix with comparable dielectric values is an effective and straightforward strategy to mitigate the field intensification effect in the ceramic/polymer nanocomposites[15,21,30]. Thus, TiO_2 with relatively low average dielectric constant is judiciously selected as dopants in the fabrication of nanocomposite dielectrics.

Figure 6d shows the E_b of these proposed nanocomposites. As seen, E_b increases with the introduction of 2.5 vol % loading of *f*-DOPA@TiO_2 NWs. Further increase of nanowire loading would give rise to the decrease of E_b. These results can be ascribed to inevitable electric field enhancement upon the polymer matrix, resulting from the large electrical mismatch between the nanowires and the polymer matrix. Even at the highest loading of 15 vol % TiO_2 NWs, these types of proposed nanocomposites can still withstand the electric field strength as high as ca. 350 MV m^{-1}. The outstanding breakdown strength of these proposed nanocomposites might be ascribed to the following reasons: (i) The comparable dielectric constant of TiO_2 NWs with the neat polymer and contributing surface functionalization by dopamine derivatives can effectively minimize the field distortion between the nanofillers and the polymer matrix[15,21,30]. (ii) The orientation of the high-aspect-ratio nanowires facilitates the formation of anisotropic polymer nanocomposite dielectrics, leading to anisotropy in the susceptibility of the nanocomposite films under the applied electric field and a lower concentration of electric field in the polymer matrix[29,61–66]. Furthermore, the growth of electrical treeing within the nanocomposites can be also restrained owing to the oriented nanowires, which benefit the generation of twisted pathways for treeing and scattering centers for the charge carriers[64–66].

In order to further validate the influence of the leakage current within the nanocomposite films towards these aforementioned properties, the current-voltage (*I*–*V*) curves of neat polymer and the presented nanocomposites are shown in Fig. 6e. These films exhibited bipolar resistive switching properties, depending on the electric field polarity when electric field was swept from 0 to +100 MV m^{-1} and then back to −100 MV m^{-1}. The leakage current densities of these nanocomposites follow a reasonable rising trend upon the increasing loading of the proposed nanowires, due to defects and voids accompanied with the incorporation of nanowires into the polymer matrix. Furthermore, the electrical resistivities shown in Fig. 6f lie in the range of 10^{11}–10^{12} Ω cm, indicating their excellent insulating property qualified for the practical applications.

Conclusions

In conclusion, mussel-inspired fluoro-dopamine (*f*-DOPA) is successfully employed to functionalize the TiO_2 NWs. The significantly improved interface compatibility and homogeneous dispersion of modified TiO_2 NWs in the P(VDF-HFP) matrix are guaranteed by the facile modification with fluoro-polydopamine. The dielectric constants of the present nanocomposites are confronted with a gradual increase upon the increasing loading of these modified nanowires, while the dielectric losses are still suppressed in comparison with the neat polymer. Moreover, the proposed nanocomposites can still withstand over the electric field of ca. 350 MV m^{-1}. Furthermore, the energy storage capabilities of the nanocomposites are also superior to the neat polymer and some of previously reported nano-TiO_2 based polymer nanocomposites. For instance, the discharged energy density of the polymer nanocomposites with 2.5 vol % *f*-DOPA@TiO_2 NWs at the applied field of 530 MV m^{-1} is 11.48 J cm^{-3}, more than three times of commercial BOPP (3.56 J cm^{-3} at 600 MV m^{-1}). A compelling high energy density of 9.12 J cm^{-3} could be achieved at a rather low electric field of 360 MV m^{-1} even with nanofiller loading as high as 15 vol %, which is nearly doubled to that of pure P(VDF-HFP) (4.76 J cm^{-3} at 360 MV m^{-1}). These results indicate that the elaborate modification of nanofillers can facilitate the subsequent performance improvement of the polymer nanocomposites. This work provides an attractive paradigm along with a unique strategy for high energy storage capability of polymer nanocomposites at both low and high electric fields.

References

1. Whittingham, M. S. Materials challenges facing electrical energy storage. *MRS Bulletin* **33,** 411–419 (2011).
2. Sarjeant, W. J., Clelland, I. W. & Price, R. A. Capacitive components for power electronics. *Proc. IEEE* **89,** 846–855 (2001).
3. Li, Q. *et al.* Flexible high-temperature dielectric materials from polymer nanocomposites. *Nature* **523,** 576–579 (2015).
4. Chu, B. *et al.* A dielectric polymer with high electric energy density and fast discharge speed. *Science* **313,** 334–336 (2006).
5. Chen, Q., Shen, Y., Zhang, S. & Zhang, Q. M. Polymer-based dielectrics with high energy storage density. *Annu. Rev. Mater. Res.* **45,** 433–458 (2015).
6. Zhu, L. & Wang, Q. Novel ferroelectric polymers for high energy density and low loss dielectrics. *Macromolecules* **45,** 2937–2954 (2012).
7. Ling, Z.-P., Zhu, J.-T., Liu, X. & Ang, K.-W. Interface engineering for the enhancement of carrier transport in black phosphorus transistor with ultra-thin high-*k* gate dielectric. *Sci. Rep.* **6,** 26609 (2016).
8. Li, J., Khanchaitit, P., Han, K. & Wang, Q. New route toward high-energy-density nanocomposites based on chain-end functionalized ferroelectric polymers. *Chem. Mater.* **22,** 5350–5357 (2010).
9. Bretos, I. *et al.* Active layers of high-performance lead zirconate titanate at temperatures compatible with silicon nano- and microelecronic devices. *Sci. Rep.* **6,** 20143 (2016).
10. Qiao, Y. *et al.* Polymers containing highly polarizable conjugated side chains as high-performance all-organic nanodielectric materials. *Adv. Funct. Mater.* **23,** 5638–5646 (2013).
11. Huang, Y., Huang, X., Schadler, L. S., He, J. & Jiang, P. Core@double-shell structured nanocomposites: A route to high dielectric constant and low loss material. *ACS Appl. Mater. Interfaces* **8,** 25496–25507 (2016).
12. Han, K. *et al.* A hybrid material approach toward solution-processable dielectrics exhibiting enhanced breakdown strength and high energy density. *Adv. Funct. Mater.* **25,** 3505–3513 (2015).
13. Li, Q. *et al.* Solution-processed ferroelectric terpolymer nanocomposites with high breakdown strength and energy density utilizing boron nitride nanosheets. *Energy Environ. Sci.* **8,** 922–931 (2015).
14. Li, Q., Han, K., Gadinski, M. R., Zhang, G. & Wang, Q. High energy and power density capacitors from solution-processed ternary ferroelectric polymer nanocomposites. *Adv. Mater.* **26,** 6244–6249 (2014).
15. Li, J. *et al.* Nanocomposites of ferroelectric polymers with TiO_2 nanoparticles exhibiting significantly enhanced electrical energy density. *Adv. Mater.* **21,** 217–221 (2009).
16. Li, J., Claude, J., Norena-Franco, L. E., Seok, S. I. & Wang, Q. Electrical energy storage in ferroelectric polymer nanocomposites containing surface-functionalized $BaTiO_3$ nanoparticles. *Chem. Mater.* **20,** 6304–6306 (2008).
17. Fredin, L. A., Li, Z., Lanagan, M. T., Ratner, M. A. & Marks, T. J. Substantial recoverable energy storage in percolative metallic aluminum-polypropylene nanocomposites. *Adv. Funct. Mater.* **23,** 3560–3569 (2013).
18. Fredin, L. A., Li, Z., Ratner, M. A., Lanagan, M. T. & Marks, T. J. Enhanced energy storage and suppressed dielectric loss in oxide core-shell-polyolefin nanocomposites by moderating internal surface area and increasing shell thickness. *Adv. Mater.* **24,** 5946–5953 (2012).
19. Li, Z. *et al. In situ* catalytic encapsulation of core-shell nanoparticles having variable shell thickness: Dielectric and energy storage properties of high-permittivity metal oxide nanocomposites. *Chem. Mater.* **22,** 5154–5164 (2010).
20. Huang, Y. *et al.* The effects of nanoparticles and organic additives with controlled dispersion on dielectric properties of polymers: Charge trapping and impact excitation. *J. Appl. Phys.* **120,** 055102/1–055102/12 (2016).
21. Dang, Z.-M., Yuan, J.-K., Yao, S.-H. & Liao, R.-J. Flexible nanodielectric materials with high permittivity for power energy storage. *Adv. Mater.* **25,** 6334–6365 (2013).
22. Liu, S., Xue, S., Xiu, S., Shen, B. & Zhai, J. Surface-modified $Ba(Zr_{0.3}Ti_{0.7})O_3$ nanofibers by polyvinylpyrrolidone filler for poly(vinylidene fluoride) composites with enhanced dielectric constant and energy storage density. *Sci. Rep.* **6,** 26198 (2016).
23. Huang, X. & Jiang, P. Core-shell structured high-k polymer nanocomposites for energy storage and dielectric applications. *Adv. Mater.* **27,** 546–554 (2015).
24. Tang, H., Lin, Y. & Sodano, H. A. Synthesis of high aspect ratio $BaTiO_3$ nanowires for high energy density nanocomposite capacitors. *Adv. Energy Mater.* **3,** 451–456 (2013).
25. Tang, H. & Sodano, H. A. Ultra high energy density nanocomposite capacitors with fast discharge using $Ba_{0.2}Sr_{0.8}TiO_3$ nanowires. *Nano Lett.* **13,** 1373–1379 (2013).
26. Tang, H., Lin, Y. & Sodano, H. A. Enhanced energy storage in nanocomposite capacitors through aligned PZT nanowires by uniaxial strain assembly. *Adv. Energy Mater.* **2,** 469–476 (2012).
27. Tang, H. & Sodano, H. A. High energy density nanocomposite capacitors using non-ferroelectric nanowires. *Appl. Phys. Lett.* **102,** 063901/1–063901/4 (2013).
28. Zhang, X. *et al.* Ultrahigh energy density of polymer nanocomposites containing $BaTiO_3$@TiO_2 nanofibers by atomic-scale interface engineering. *Adv. Mater.* **27,** 819–824 (2015).
29. Hu, P. *et al.* Topological-structure modulated polymer nanocomposites exhibiting highly enhanced dielectric strength and energy density. *Adv. Funct. Mater.* **24,** 3172–3178 (2014).
30. Xu, N. *et al.* Significantly enhanced dielectric performance of poly(vinylidene fluoride-co-hexafluoropropylene)-based composites filled with hierarchical flower-like TiO_2 particles. *ACS Appl. Mater. Interfaces* **7,** 27373–27381 (2015).
31. Pujari, S. P., Scheres, L., Marcelis, A. T. M. & Zuilhof, H. Covalent surface modification of oxide surfaces. *Angew. Chem., Int. Ed.* **53,** 6322–6356 (2014).
32. Haensch, C., Hoeppener, S. & Schubert, U. S. Chemical modification of self-assembled silane based monolayers by surface reactions. *Chem. Soc. Rev.* **39,** 2323–2334 (2010).
33. Xie, L., Huang, X., Wu, C. & Jiang, P. Core-shell structured poly(methyl methacrylate)/$BaTiO_3$ nanocomposites prepared by *in situ* atom transfer radical polymerization: A route to high dielectric constant materials with the inherent low loss of the base polymer. *J. Mater. Chem.* **21,** 5897–5906 (2011).
34. Xie, L., Huang, X., Huang, Y., Yang, K. & Jiang, P. Core@double-shell structured $BaTiO_3$-polymer nanocomposites with high dielectric constant and low dielectric loss for energy storage application. *J. Phys. Chem. C* **117,** 22525–22537 (2013).
35. Xie, L., Huang, X., Yang, K., Li, S. & Jiang, P. "Grafting to" route to PVDF-HFP-GMA/$BaTiO_3$ nanocomposites with high dielectric constant and high thermal conductivity for energy storage and thermal management applications. *J. Mater. Chem. A* **2,** 5244–5251 (2014).
36. Yang, K. *et al.* Core-shell structured polystyrene/$BaTiO_3$ hybrid nanodielectrics prepared by *in situ* RAFT polymerization: A route to high dielectric constant and low loss materials with weak frequency dependence. *Macromol. Rapid Commun.* **33,** 1921–1926 (2012).
37. Yang, K., Huang, X., Huang, Y., Xie, L. & Jiang, P. Fluoro-polymer@$BaTiO_3$ hybrid nanoparticles prepared via RAFT polymerization: Toward ferroelectric polymer nanocomposites with high dielectric constant and low dielectric loss for energy storage application. *Chem. Mater.* **25,** 2327–2338 (2013).
38. Yang, K. *et al.* Combining RAFT polymerization and thiol-ene click reaction for core-shell structured polymer@$BaTiO_3$ nanodielectrics with high dielectric constant, low dielectric loss and high energy storage capability. *ACS Appl. Mater. Interfaces* **6,** 1812–1822 (2014).

39. Zhu, M. *et al.* Energy storage in ferroelectric polymer nanocomposites filled with core-shell structured polymer@$BaTiO_3$ nanoparticles: Understanding the role of polymer shells in the interfacial regions. *ACS Appl. Mater. Interfaces* **6,** 19644–19654 (2014).
40. Lee, H., Dellatore, S. M., Miller, W. M. & Messersmith, P. B. Mussel-inspired surface chemistry for multifunctional coatings. *Science* **318,** 426–430 (2007).
41. Lee, H., Lee, B. P. & Messersmith, P. B. A reversible wet/dry adhesive inspired by mussels and geckos. *Nature* **448,** 338–341 (2007).
42. d'Ischia, M., Napolitano, A., Ball, V., Chen, C.-T. & Buehler, M. J. Polydopamine and eumelanin: From structure-property relationships to a unified tailoring strategy. *Acc. Chem. Res.* **47,** 3541–3550 (2014).
43. Dreyer, D. R., Miller, D. J., Freeman, B. D., Paul, D. R. & Bielawski, C. W. Perspectives on poly(dopamine). *Chem. Sci.* **4,** 3796–3802 (2013).
44. Ye, Q., Zhou, F. & Liu, W. Bioinspired catecholic chemistry for surface modification. *Chem. Soc. Rev.* **40,** 4244–4258 (2011).
45. Lynge, M. E., van der Westen, R., Postma, A. & Staedler, B. Polydopamine-a nature-inspired polymer coating for biomedical science. *Nanoscale* **3,** 4916–4928 (2011).
46. Rodenstein, M., Zurcher, S., Tosatti, S. G. P. & Spencer, N. D. Fabricating chemical gradients on oxide surfaces by means of fluorinated, catechol-based, self-assembled monolayers. *Langmuir* **26,** 16211–16220 (2010).
47. Hong, D. *et al.* Mussel-inspired, perfluorinated polydopamine for self-cleaning coating on various substrates. *Chem. Commun.* **50,** 11649–11652 (2014).
48. Manolakis, I., Noordover, B. A. J., Vendamme, R. & Eevers, W. Novel *L*-DOPA-derived poly(ester amide)s: Monomers, polymers, and the first *L*-DOPA-functionalized biobased adhesive tape. *Macromol. Rapid Commun.* **35,** 71–76 (2014).
49. Pugh, C., Singh, A., Samuel, R. & Bernal Ramos, K. M. Synthesis of hyperbranched polyacrylates by a chloroinimer approach. *Macromolecules* **43,** 5222–5232 (2010).
50. Wang, G., Huang, X. & Jiang, P. Tailoring dielectric properties and energy density of ferroelectric polymer nanocomposites by high-*k* nanowires. *ACS Appl. Mater. Interfaces* **7,** 18017–18027 (2015).
51. Dang, Z.-M. *et al.* Fabrication and dielectric characterization of advanced $BaTiO_3$/polyimide nanocomposite films with high thermal stability. *Adv. Funct. Mater.* **18,** 1509–1517 (2008).
52. Dang, Z.-M., Xu, H.-P. & Wang, H.-Y. Significantly enhanced low-frequency dielectric permittivity in the $BaTiO_3$/poly(vinylidene fluoride) nanocomposite. *Appl. Phys. Lett.* **90,** 012901/1–012901/3 (2007).
53. Huang, X., Xie, L., Jiang, P., Wang, G. & Liu, F. Electrical, thermophysical and micromechanical properties of ethylene-vinyl acetate elastomer composites with surface modified $BaTiO_3$ nanoparticles. *J. Phys. D: Appl. Phys.* **42,** 245407/1–245407/10 (2009).
54. Rahimabady, M., Mirshekarloo, M. S., Yao, K. & Lu, L. Dielectric behaviors and high energy storage density of nanocomposites with core-shell $BaTiO_3$@TiO_2 in poly(vinylidene fluoride-hexafluoropropylene). *Phys. Chem. Chem. Phys.* **15,** 16242–16248 (2013).
55. Li, Y. *et al.* Large dielectric constant and high thermal conductivity in poly(vinylidene fluoride)/barium titanate/silicon carbide three-phase nanocomposites. *ACS Appl. Mater. Interfaces* **3,** 4396–4403 (2011).
56. Mijovic, J., Sy, J.-W. & Kwei, T. K. Reorientational dynamics of dipoles in poly(vinylidene fluoride)/poly(methyl methacrylate) (PVDF/PMMA) blends by dielectric spectroscopy. *Macromolecules* **30,** 3042–3050 (1997).
57. Chung, T. C. M. Functionalization of polypropylene with high dielectric properties: Applications in electric energy storage. *Green Sustainable Chem.* **2,** 29–37 (2012).
58. Zhang, X. *et al.* Giant energy density and improved discharge efficiency of solution-processed polymer nanocomposites for dielectric energy storage. *Adv. Mater.* **28,** 2055–2061 (2016).
59. Hu, P. *et al.* Highly enhanced energy density induced by hetero-interface in sandwich-structured polymer nanocomposites. *J. Mater. Chem. A* **1,** 12321–12326 (2013).
60. Chen, Q., Wang, Y., Zhou, X., Zhang, Q. M. & Zhang, S. High field tunneling as a limiting factor of maximum energy density in dielectric energy storage capacitors. *Appl. Phys. Lett.* **92,** 142909/1–142909/3 (2008).
61. Wang, Z., Nelson, J. K., Hillborg, H., Zhao, S. & Schadler, L. S. Dielectric constant and breakdown strength of polymer composites with high aspect ratio fillers studied by finite element models. *Compos. Sci. Technol.* **76,** 29–36 (2013).
62. Wang, Z. *et al.* Effect of high aspect ratio filler on dielectric properties of polymer composites: A study on barium titanate fibers and graphene platelets. *IEEE Trans. Dielectr. Electr. Insul.* **19,** 960–967 (2012).
63. Song, Y. *et al.* Significant enhancement in energy density of polymer composites induced by dopamine-modified $Ba_{0.6}Sr_{0.4}TiO_3$ nanofibers. *Appl. Phys. Lett.* **101,** 152904/1–152904/3 (2012).
64. Hu, P. *et al.* Largely enhanced energy density in flexible p(VDF-TrFE) nanocomposites by surface-modified electrospun $BaSrTiO_3$ fibers. *J. Mater. Chem. A* **1,** 1688–1693 (2013).
65. Song, Y. *et al.* Enhanced dielectric and ferroelectric properties induced by dopamine-modified $BaTiO_3$ nanofibers in flexible poly(vinylidene fluoride-trifluoroethylene) nanocomposites. *J. Mater. Chem.* **22,** 8063–8068 (2012).
66. Song, Y. *et al.* Improving the dielectric constants and breakdown strength of polymer composites: Effects of the shape of the $BaTiO_3$ nanoinclusions, surface modification and polymer matrix. *J. Mater. Chem.* **22,** 16491–16498 (2012).

Acknowledgements

This work was supported by National Natural Science Foundation of China (nos 51522703, 51277117, 51477096) and the Special Fund of the National Priority Basic Research of China under Grant 2014CB239503. Xingyi Huang also thanks the 2013 SMC Excellent Young Faculty Award of Shanghai Jiao Tong University and Shanghai Pujiang Program under Grant PJ14D018. The authors are also grateful to researchers in the Instrument Analysis Center of Shanghai Jiao Tong University for their help of XPS measurements using an Axis UltraDLD spectrometer (Shimadzu-Kratos Analytical Ltd, UK) in material analysis.

Author Contributions

X.Y.H. supervised the work. W.G.Y. wrote the manuscript. All authors discussed the results. All authors reviewed and commented on the manuscript. All authors agree the contents of the manuscript.

Additional Information

Supplementary information accompanies this paper at http://www.nature.com/srep

Competing financial interests: The authors declare no competing financial interests.

How to cite this article: Wang, G. *et al.* Mussel-inspired Fluoro-Polydopamine Functionalization of Titanium Dioxide Nanowires for Polymer Nanocomposites with Significantly Enhanced Energy Storage Capability. *Sci. Rep.* **7**, 43071; doi: 10.1038/srep43071 (2017).